Biomaterials Science

ROYAL SOCIETY OF CHEMISTRY

PAPER

View Article Online
View Journal | View Issue

Cite this: *Biomater. Sci.*, 2025, **13**, 6085

Bioactive coating with clindamycin, VEGF-165, and TGF-β1 for supporting bone tissue regeneration

Dagmara Słota, *[a] Aleksandra Szwed-Georgiou, [b] Marcin Włodarczyk,[b] Agnieszka Krupa,[b] Karolina Rudnicka, [b] Karina Niziołek,[a] Bartłomiej Kryszak,[c] Konrad Szustakiewicz [c] and Agnieszka Sobczak-Kupiec[d]

The growing demand for implantable devices, implants, and plastic surgery is a major factor driving the growth of the global biomaterials market. Both new materials and opportunities to enhance the properties of existing solutions are being explored. One such approach involves coating existing materials with bioactive layers to provide additional functions. In this study, a bioactive coating was developed in an environmentally friendly and cost-effective manner, using polyethylene glycol (PEG), polyvinylpyrrolidone (PVP), hydroxyapatite (HAp), collagen (COL), and glutathione (GSH). The coating demonstrated the ability to release the antibiotic clindamycin, the vascular endothelial growth factor-165 (VEGF-165), which promotes angiogenesis, and the transforming growth factor-β1 (TGF-β1), which provides anti-inflammatory properties. The physicochemical properties of the coating were evaluated, and its *in vivo* integration with natural bone tissue was assessed using a rat skull bone defect model in adult Wistar rats (Rattus norvegicus). It was demonstrated that VEGF-165 and TGF-β1 were released within 24 hours at approximately 30% each, a dose capable of producing a therapeutic effect. The *in vivo* results suggest that incorporating growth factors into the composite coating significantly promotes mineralization at the site of injury. Our coating has the potential to support bone tissue regeneration through the synergistic effects of proteins; however, further studies are required.

Received 24th April 2025,
Accepted 31st July 2025

DOI: 10.1039/d5bm00637f

rsc.li/biomaterials-science

Introduction

The global biomaterials market continues to grow, with increases driven by growing funding for regenerative and personalized medicine, the use of biomaterials in various therapeutic areas, as well as rising demand for implantable devices or plastic surgery. Biomaterials for bone tissue include implants for defects, biocomposites, endporpotes or coatings. The last ones are particularly interesting as they can provide additional functions without changing the underlying parameters they cover, such as a personalized 3D printed defect or endoprosthesis.[1,2] Orthopaedic injuries involving the aforementioned biomaterials represent a significant public health problem worldwide and a heavy burden of disability or suffering for patients. Globally, there has been a major increase in the number of musculoskeletal disorders that require surgical interventions involving the use of permanent, temporary or biodegradable medical devices. Statistics from 1990 indicate 221 million patients affected by orthopaedic conditions, while in 2020, as many as 494 million patients were reported, which represents an increase of 123.4%. It is important to note that the success of a clinician's intervention, depends largely on the character of the chosen device and its parameters, which will determine the biological response. For this reason, more and more bioactive biocomposites are designed.[3] However, in the process of developing new materials, it is crucial to consider not only their functional properties but also their impact on the natural environment. In the face of ongoing climate change and ecosystem degradation, it is essential to employ sustainable synthesis methods that minimize raw material and energy consumption while reducing waste.[4–6]

Ceramic-polymer biocomposites are a modern group of materials dedicated to biomedical engineering applications, particularly in bone tissue implantology. They are multiphase systems combining the properties of ceramic inorganic materials, most often calcium phosphates such as hydroxyapatite (HAp), with polymers, both natural (*e.g.* collagen) and

[a]*Cracow University of Technology, CUT Doctoral School, Faculty of Materials Engineering and Physics, Department of Materials Science, 37 Jana Pawła II Av., 31-864 Krakow, Poland. E-mail: dagmara.slota@pk.edu.pl*
[b]*University of Lodz, Faculty of Biology and Environmental Protection, Department of Immunology and Infectious Biology, 12/16 Banacha St, 90-237 Łódź, Poland*
[c]*Department of Polymer Engineering and Technology, Faculty of Chemistry, Wroclaw University of Science and Technology, Wyb. Wyspianskiego 27, 50-370 Wroclaw, Poland*
[d]*Cracow University of Technology, Faculty of Materials Engineering and Physics, Department of Materials Science, 37 Jana Pawła II Av., 31-864 Krakow, Poland*

of synthetic origin (*e.g.* polyvinylpyrrolidone (PVP) or polyethylene glycol (PEG)).[7–9] The ceramic component provides bioactivity, understood as the ability to form bonds with natural bone tissue, as well as high mechanical compressive strength to the composites. Moreover, it stimulates bone-forming cells to proliferate.[10–12] On the other hand, the polymer component improves flexibility, reduces the brittleness of the ceramic, and enables controlled release of active agents such as growth factors such as vascular endothelial growth factor, transforming growth factor or drugs. As a result of these properties, ceramic-polymer biocomposites can be used in bone fillings, scaffolds and as implant coatings[13–15]

A key challenge in material design is optimizing mechanical, physicochemical as well as biocompatibility properties. It is important to achieve a balance between the durability of the material, its performance as well as its ability to promote regenerative processes.[16,17] Furthermore, it is necessary to confirm the effectiveness and safety of potential biomaterials in *in vivo* studies, which provide the necessary information on their behaviour in a complex biological environment. In the case of class III medical devices *e.g.* all implantable materials, such preclinical studies are required, as potential toxicity or other risks can be excluded.[18] *In vivo* studies enable assessment of the biocomposite's integration with natural bone tissue or the degree of induction of osteogenesis.[19,20] Thanks to such analyses, it is possible to tailor the properties of biocomposites to individual patient requirements, which are also particularly important in the context of personalizing materials in terms of the amount of active substances released, since the dose will naturally be different for an adult and a child.

In this work, a ceramic-polymer coating capable of releasing vascular endothelial growth factor (VEGF) and transforming growth factor-β (TGF-β) from between polymer chains was analysed thoroughly. These two proteins were chosen because of their biological properties. VEGF is a highly pleiotropic protein with both vascular as well as extravascular functions. Primarily, it is known as an angiogenesis factor that, has the ability to rebuild blood vessels.[21] Furthermore, it induces proliferation, migration as well as capillary morphogenesis of endothelial cells.[22] Depending on the number of amino acid residues, there are several isoforms of this protein, of which VEGF121, -165, -189 and -206 are the most dominant. Apart from their influence on the processes of angiogenesis, they also affect the development of the nervous system.[23,24] TGF-β is an anti-inflammatory factor and a key regulator of many cellular functions, including cellular immunity. It maintains immune homeostasis and prevents autoimmunity.[25] The effects of this protein on osteoblasts is also proven, resulting in increased differentiation, which includes the secretion of bone matrix proteins and subsequent mineralization.[26]

Despite numerous advances in the development of materials engineering or ceramic-polymer biomaterials, there is still a lack of bioactive coatings capable of delivering multiple biological agents in a controlled manner while maintaining adequate mechanical properties, biocompatibility and biodegradability. Furthermore, many proposed systems have not been validated *in vivo*, limiting their clinical relevance and hindering implementation. The research presented in this manuscript seeks to fill this gap by proposing a multifunctional composite coating that combines hydroxyapatite with a PVP : PEG matrix, enabling dual release of VEGF and TGF-β, the drug, and allowing direct application to solid surfaces *via* photocrosslinking, while also subscribing to the concept of sustainable production.

In this study, we present a new, previously unproposed strategy for obtaining and applying a bioactive coating for covering solid materials for the treatment of bone regeneration. The innovative character of this work lies not only in the crosslinking method itself, which has been explored in other biomedical contexts, but also in the integration of this approach into a ceramic-polymer material that supports dual growth factor as well as drug release and has been biologically validated *in vivo*. To our knowledge, this is the first report of such a coating composition, structure, and application method being tested in an animal model, thus providing a significant step toward clinical translation in bone tissue regeneration For the first time, coatings obtained by photocrosslinking with such chemical composition and biological properties are presented.

Materials and methods

Reagents

Reagents for the synthesis of ceramics phase, such as sodium phosphate dibasic (Na_2HPO_4), calcium acetate monohydrate ($Ca(CH_3CO_2)_2{\cdot}H_2O$) and ammonia solution ($NH_4OH$, 25%), were purchased from Sigma-Aldrich (Darmstadt, Germany). Medical grade poly(L-lactide) (PLLA), Resomer L210S (M_n = 304 020 g mol^{-1}, PDI = 1.96, 100% L-lactide unit fraction) from Evonik (Essen, Germany) was used for composite plates preparation. All polymers, along with other components required for the synthesis of the coatings, including polyvinylpyrrolidone (PVP), polyethylene glycol (PEG), poly(ethylene glycol) diacrylate (PEGDA) with a molecular weight of 5752-hydroxy-2-methylpropiophenone (97%), L-glutathione peptide (reduced, 98%) (GSH), and collagen derived from bovine Achilles tendon (COL), were also sourced from Sigma-Aldrich (Darmstadt, Germany). Clindamycin hydrochloride, one of the active ingredient chosen for coating modification, was also obtained from Sigma-Aldrich (Darmstadt, Germany). The active ingredients for the coating modification, *i.e.* Recombinant Human VEGF-165 and Recombinant Human TGF-β1, were purchased from Shenandoah Biotechnology (Warminster, U.S.) and Merck (Darmstadt, Germany), respectively. The Human VEGF Elisa Kit and Human TGF-β1 ELISA Kit from Invitrogen by Thermo Fisher Scientific (Vienna, Austria) were used sequentially for their determination after *in vitro* release.

PLLA/HAp plates preparation

The first stage involved preparing the materials for processing. Synthetic HAp with a Ca/P molar ratio of 1.67 was used.

Details on the preparation of HAp are provided in the SI (subsections 1–4). The post-synthetic HAp suspension was decanted. The resulting sediment was frozen at −40 °C and then freeze-dried at −53 °C under a vacuum (below 10 mbar) using a FreeZone 2.5 Liter Benchtop Freeze Dryer (Labconco, USA). The HAp powder was then calcined in an electric furnace at 600 °C for 3 hours, while the PLLA was dried at 70 °C for 24 hours. Finally, the materials were weighed, thoroughly mixed at a polymer-to-filler weight ratio of 7 : 3, and prepared for further processing.

A processing procedure was selected to ensure good dispersion of HAp in the PLLA matrix, as well as dimensional stability and product repeatability.[27] To effectively incorporate the HAp filler into the polymer, the prepared formulation was processed by co-rotating twin-screw extrusion. A Thermo Fisher Scientific (Waltham, USA) twin-screw extruder (D = 20 mm, L/D = 40) equipped with special mixing zones was used. The material was processed at a screw speed of 200 rpm and a set temperature of 200 °C across all heating zones. The extrudate was cooled on an air track, wound on a winder (Thermo Fisher Scientific, Waltham, USA) and regranulated using a Brabender (Duisburg, Germany) pelletizer. The composite granules were subsequently injection molded using a BOY XS micro-injection molding machine (Dr Boy GmbH & Co. KG, Neustadt-Fernthal, Germany). The process was performed with a barrel temperature of 220 °C, a flow channel temperature of 200 °C, an injection pressure of 250 bar, a cooling time of 15 seconds, and a cooling temperature of 50 °C. The injection molding process produced plate-shaped samples with dimensions of 35 mm × 35 mm and a thickness of 2 mm.

The final forming process was carried out using CNC milling with an ATMSolutions Basic Mill (Warsaw, Poland), controlled by Mach 3 CNC Controller software and equipped with a 1 mm diameter end mill. The cylinders, made from injection-molded plates, were 2 mm high and 3.8 mm in diameter. Each cylinder had a symmetrically oriented hole in the base, milled to a depth of 1 mm and a diameter of 3.0 mm. They provided a base in the form of plates on which the bioactive coatings were applied.

Preparation of coatings

Additional information regarding the preparation of coatings is presented in the SI (subsection 5). Fig. 1A schematically presents the process of obtaining coatings. Coatings composition is presented in Table 1. 200 µl of the mixture was deposited on a PLLA/HAp plate and crosslinked. The materials were obtained by UV photocrosslinking process using a suitable crosslinking agent and photoinitiator. The sample was irradiated for 4 minutes at an irradiation power of 0.8 J cm^{-2}. An example of the resulting coating applied to a PLLA/HAp pad, ready for implantation into an animal model is presented in Fig. 1B.

The proposed material obtaining method is environmentally friendly, does not generate by-products that would require disposal and allows for full incorporation of all reagents used during synthesis. Coatings modified with growth factors were

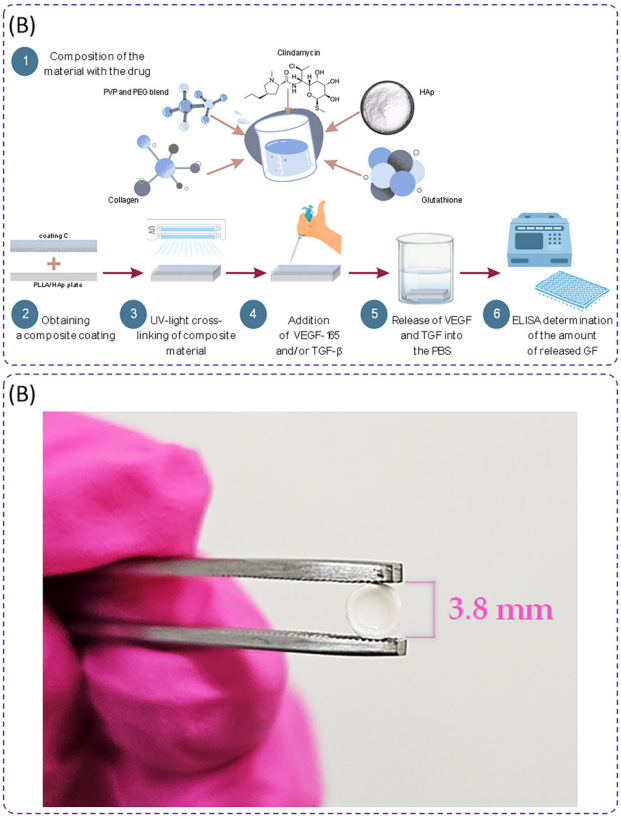

Fig. 1 (A) Schematic of the process of obtaining and modifying the coating with GF proteins. (B) Coating applied to a PLLA/HAp plate ready for *in vivo* implementation.

Table 1 Composition of coatings indicating basic differences in formulation

Coating symbol	Coating C	Coating 4	Coating C/GF
PVP 15% [µL]	100		
PEG 15% [µL]	100		
COL [mg]	0.8		
GSH [mg]	40		
HAP [mg]	10		
Clindmycin [mg]	—	0.5	—
VEGF-165 [µg]	—	—	100
TGF-β1 [µg]	—	—	100

produced as follows. An aqueous solution of VEGF-165 and an aqueous solution of TGF-β1 were prepared in order to reconstruct proteins. Solutions of VEGF-165 and/or TGF-β1 were then dripped onto the surface of the cross-linked coating so that 100 µg of the selected protein was present in the material. Based on our previous work the coating thickness in this study was assumed to be approximately 600 µm, which is considered suitable for bone tissue regeneration.[28] We acknowledge that depending on the type of implant *e.g.*, a 3D-printed material designed to fill a bone defect or a metallic endoprosthesis – some variability in coating thickness may arise due to differences in geometry and application conditions. Nevertheless,

the method enables full reagent utilization without generating by-products, supporting its environmentally responsible profile.

Determination of sedimentation rate

The process of obtaining composite coatings was carried out under UV light using a photocrosslinking process that occurred over a period of 4 minutes. In order to avoid excessive sedimentation of the powder in the aqueous solution of the polymers, an analysis of the sedimentation rate of HAp powder in different concentrations of PVP/PEG was carried out. A polymer ratio of 1 : 1 (PVP : PEG) and its aqueous concentrations of 0%, 5%, 10%, 15%, 20% and 25% were proposed. The analysis was carried out using a MultiScan MS20 DataPhysics Instruments (Filderstadt, Germany). Measurements were conducted for 10 minutes, performing 20 scans at a time interval of 12 seconds.

Fourier-transform infrared spectroscopy analysis

The composition of coating composite materials has been selected and studied previously,[28,29] however, the mechanism of the occurring photocrosslinking process has not been adequately investigated so far. In order to clarify the phenomena occurring, the base composition in the form of a PVP/PEG blend was analysed using Fourier transform infrared spectroscopy. Analysis was also performed for coatings modified with clindamycin, VEGF and TGF to determine whether the addition of the active ingredient affects the overall system. The study was performed using a Nicolet iS5 FT-IR spectrometer equipped with an iD7 ATR detector (Thermo Scientific, Loughborough, UK). The measurement was carried out at room temperature, in the range from 4000 to 400 cm^{-1}. For each sample, a total of 32 scans were carried out at a resolution of 4.0 cm^{-1}.

Morphology analysis

The coating materials were imaged by scanning electron microscopy (SEM) to determine whether additions of active ingredients affect the morphology of the biomaterials. The interior of the coatings was examined. Prior to measurement, the coatings were thoroughly dried, bonded to carbon pads for immobilization, and then coated with a layer of nano-gold using a DII-29030SCTR Smart Coater sputtering device (JEOL Ltd, MA, USA). A JEOL IT200 microscope (JEOL Ltd, MA, USA) was used for imaging. The device is equipped with an energy-dispersive X-ray spectroscopy (EDX) system detector, with which elemental analysis and mapping of elements on the surface were carried out. Elemental analysis was carried out by determining mass percentage (%M.) as well as atomic percentage (%At.). The measurements were performed at ×500 magnification.

TGF-β1 release test

The TGF-β1-modified sample was incubated in 1 mL PBS. After 24 h, a 100 μL sample of incubation fluid was collected and protein determination was performed. TGF-β1 detection was performed using the corresponding Invitrogen Thermo Fisher Scientific ELISA kit and its protocol.[30] Reconstitution of the human TGF standard to a concentration of 4 ng mL^{-1} was performed. A series of dilutions of the standards to 2000 pg mL^{-1}, 1000 pg mL^{-1}, 500 pg mL^{-1}, 250 pg mL^{-1}, 125 pg mL^{-1}, 63 pg mL^{-1} and 31 pg mL^{-1} were then prepared. Then 20 μL of the sample was mixed with 180 μL Assay Buffer and 20 μL of 1 N HCl and allowed to stand for 1 h. After this time, 20 μL of 1 N NaOH was added and the wells were washed with Wash Buffer. 60 μL Assay Buffer was added and allowed to stand at room temperature for 2 h. During this time, the plate was continuously shaken. After this time, the plate was washed and 100 μL Biotin-conjugate was added. It was again shaken for 1 h, after which it was washed and 100 μL Streptavidin-HRP was added and again shaken for 1 h. Then 100 μL TMB Substrate Solution was washed and pipetted. Then, plate was incubated for 30 minutes in the dark, monitoring periodically the optical density for standard 1 at 620 nm, using an ELISA Microplate Reader, BioTek 800 TS (Winooski, Vermont, U.S). When it reached a value above 0.9, 100 μL of stop solution was added. Absorbance was read at 450 nm using the same device as mentioned above.

VEGF release test

The VEGF-165-modified sample was incubated in 1 mL PBS. After 24 h, a 1 μL sample of incubation fluid was collected and protein determination was performed. VEGF-165 detection was performed using the corresponding Invitrogen Thermo Fisher Scientific ELISA kit and its protocol.[31] The human VEGF standard was reconstituted to a concentration of 10 000 pg mL^{-1} and then diluted sequentially to concentrations of 1500 pg mL^{-1}, 750 pg mL^{-1}, 188 pg mL^{-1}, 93.8 pg mL^{-1}, and 23.4 pg mL^{-1} to obtain a series of standards. The Streptavidin-HRP solution was then prepared. In the first step, the procedure leading to antigen binding was carried out. 50 μL of Incubation Buffer, 100 μL of appropriate standards, 50 μL of Standard Dilueted Buffer and 50 μL of sample were added to individual wells of the 96-well plate. After 2 hours, the plate was washed with Wash Buffer and 100 μl of Biotin conjugate was added. After 1 hour, the plate was rinsed again and 100 μl of Streptavidin-HRP was added. This was allowed to stand for 30 minutes and washed again using a Wash Buffer. In the next step, 100 μl of Stabilized Chromogen was added and the color of the wells was observed to change to blue. This was incubated for 30 minutes in the dark. After this time, 100 μL Stop Solution was added to each well and the color change from blue to yellow was observed. Absorbance was read at 450 nm, using a ELISA Microplate Reader, BioTek 800 TS (Winooski, Vermont, U.S). The entire procedure was conducted at room temperature.

In vivo study on the application of biomaterials in a rat skull bone defect model

Adult rats (*Rattus norvegicus*, Wistar breed), weighing at least 220 g, aged at least 10 weeks, were used for the study. The rats were from the in-house breeding facility of the Department of

Biology and Environmental Protection at the University of Lodz. Permission to perform *in vivo* experiments (34/LB240/2022) was granted by the Local Animal Ethics Committee at the Medical University of Lodz, based on the results of *in vitro* evaluation of biocomposites, with a particular emphasis on cytocompatibility testing, as presented in our previous study.[32] The experiment included three groups, one of which contained a reference composite – coating C, and two groups contained modified composites: coating 4 and coating C/GF. The control group comprised animals that did not undergo implantation of any biomaterial, serving as a baseline for physiological responses. After 8 weeks, the animals were euthanized for blood collection (obtaining serum) and isolation of skulls with implanted biomaterials. Concentrations of the cytokines: IL-1β, IL-10, TNF-α and osteopontin (OPN) in serum samples were measured by immunoenzymatic ELISA (R&D Systems, Minneapolis, MN, USA) according to the manufacturer's instructions and as described by Słota *et al.*, 2024.[32] The assay sensitivity thresholds were 31.2 pg mL^{-1} for IL-1β and 62.5 pg mL^{-1} for IL-10, TNF-α and OPN. Absorbance at 450 nm for standards nd samples across serial dilutions was measured using a Multiskan EX microplate reader (Thermo Fisher Scientific, USA), and biomarker concentrations were calculated using GainData (Arigo Biolaboratories, **https://www.arigobio.com/elisa-analysis**). Standard curve was generated by fitting the data to a 4-parameter logistic (4PL) curve. Statistical analysis was performed using GraphPad Prism. The Kruskal–Wallis test was used to assess group differences, followed by Dunn's multiple comparisons test. Differences were considered statistically significant at $p < 0.05$.

Results and discussion

In order to select the appropriate concentration of PVP/PEG solution to form the base of the final composite coatings, the stability of the HAp ceramic phase in the polymer was evaluated. For this purpose, the migration front was determined as a function of time (Fig. 2A). The results obtained demonstrate the differences between the stability of the HAp suspensions tested.

For a concentration of 5% and distilled water (0%), the curves overlap, and the flattening of the migration front occurs a little later. For the highest concentration of 25%, the obtained curve is jagged, which may suggest that the polymer mixture was not completely homogeneous and the suspended powders did not sediment uniformly in it. It is significant that already at the stage of solution preparation, some dissolution difficulties were observed for this concentration.

Fig. 2B demonstrates the procedure for measuring sedimentation rates. The segregation process was analysed by measuring light intensity with temporal and positional resolution. Fig. 2C presents vials of HAp powder at different aqueous concentrations of PVP : PEG polymers. The results of the analysis of the sedimentation rate of HAp in PVP/PEG solutions of different concentrations are presented in Table 2. Based on the

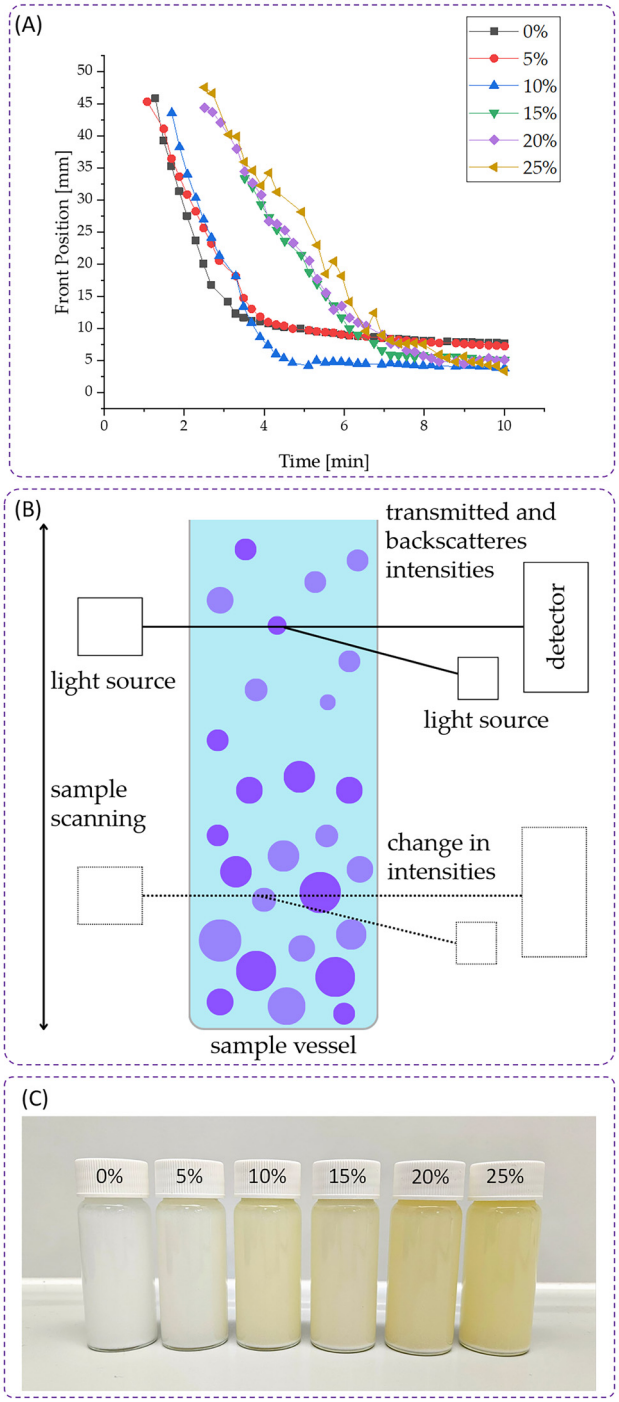

Fig. 2 (A) Migration front as a function of time for HAp powders in PVP/PEG aqueous solutions with different concentrations.(B) Schematic of the procedure for measuring the sedimentation rate. (C) Samples of ceramics in uncrosslinked polymer solution.

given values, it can be indicated that the concentration of polymer solutions affects the sedimentation process. The value obtained for the highest polymer concentration equals −10.19 ± 1.07 mm min^{-1}, and is practically three times lower than for distilled water (0%) alone. Based on the data obtained, the concentration chosen for further study was 15%. This concen-

Table 2 Sedimentation rate of HAp powder in PVP/PEG solutions of different concentrations

PVP/PEG [%]	Sedimentation rate [mm min^{-1}]
0	−35.59 ± 7.95
5	−32.59 ± 1.07
10	−24.4 ± 0.28
15	−16.25 ± 0.07
20	−12.55 ± 4.66
25	−10.19 ± 1.07

tration was found to offer a favorable balance between stabilizing ability and practical usability. At this concentration, the PVP : PEG polymers dissolved efficiently, and the HAp particles were evenly distributed, resulting in a homogeneous suspension. In contrast, higher concentrations, 20% and particularly 25% required more time and energy to dissolve and displayed visible heterogeneities during preparation. Moreover, preliminary assessments of the final UV-crosslinked coatings indicated that formulations with 20% polymer content yielded stiffer and less flexible materials compared to the 15% ones, likely due to increased crosslink density. Considering the intended application in bone tissue engineering, where moderate elasticity is beneficial, the 15% concentration was selected for further work as a compromise between colloidal stability, processability, and mechanical suitability.

The composition of coating composite materials has been selected and studied previously.[28,29,32] However, the mechanism of the occurring photocrosslinking process has not been adequately investigated so far. In order to clarify the phenomena occurring, the base composition in the form of a PVP/PEG/PEGDA blend, at PVP and PEG concentration of 15% was analyzed using Fourier transform infrared spectroscopy.

Analysis was carried out on samples of pure polymers, as well as the crosslinking agent PEGDA in crosslinked and uncrosslinked forms. The photoinitiator used was 2-hydroxy-2-methylpropiophenone. The obtained spectra are presented in Fig. 3A. Upon exposure to UV radiation, the photoinitiator dissociates into two highly reactive radicals. These attack the –C═C– double bond, which are found in PEGDA. This is evidenced by the complete disappearance of the absorption band characteristic of this bond at 1622 cm^{-1} (marked with a circle in the Fig. 3). Thus, the –C–C– covalent bond is formed, resulting in a three-dimensional network of polymer chains[33,34] For the cross-linked PVP/PEG/PEGDA polymer blend, this phenomenon is not visible because of the presence of a very strong signal that comes from the –C═O carbonyl group from PVP at 1658 cm^{-1}.[35] For the cross-linked PVP/PEG/PEGDA sample, changes in the intensity of the bands in the 3000–3500 cm^{-1} range are also observed, while they are clearly evident for the pure components, therefore may indicate interactions between the components in the matrix. It can be concluded that the formation of the materials was carried out PEGDA radical crosslinking.

The radical crosslinking presented in this work was enabled by the use of a UV light source, which also served as

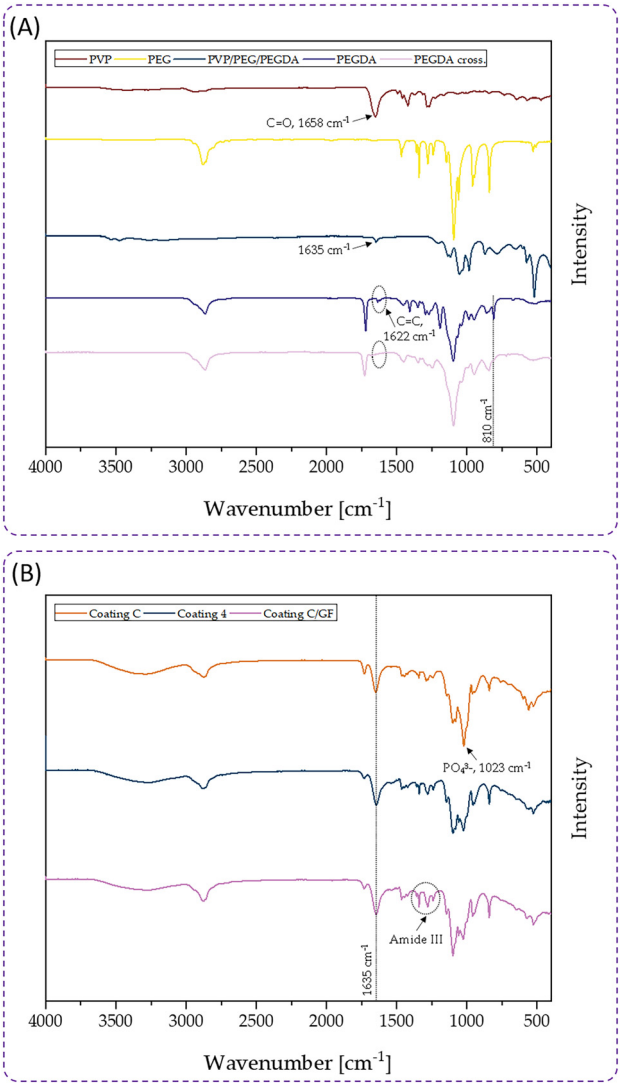

Fig. 3 (A) ATR FT-IR spectra of the individual components and the developed base polymer composition. (B) ATR FT-IR spectra of the obtained coatings.

an indicator of the process. For this reason, particular attention was given to the topic of photcrosslinking. Compared to conventional chemical crosslinking, photopolymerization offers a more sustainable approach. By significantly reducing the consumption of chemical reagents typically used in crosslinking reactions, this method contributes to the overall minimization of the carbon footprint. These advantages highlight the potential of the proposed method for biomedical applications, particularly in the development of implant coatings aimed at enhancing tissue regeneration while minimizing environmental impact.

Based on the obtained spectra, it was concluded that the resulting photocrosslinking interactions are hydrogen bonds that create an interpenetrating polymer network (IPN).[36] The occurrence of hydrogen interaction was confirmed on the basis of the peak position of the carbonyl group, which shifted gently

towards smaller values. For the PVP/PEG/PEGDA blend, the value is 1635 cm^{-1}, while for pure PVP the signal is observed at 1658 cm^{-1}. The conversion of the double bond to a single one is also confirmed by the absence of a signal at 810 cm^{-1} for PEGDA cross. Which occurs for pure PEGDA and corresponds to the –C–H bond (marked in the Fig. 3A with a dashed line).[37] Based on the above information, Fig. 4 presents the proposed polymer network formation mechanism. It is considered that the polymer networks formed in this way are a good material for carrying active substances, since they can encapsulate biomolecules in their structure between polymer chains.[38]

The spectra of the base coating and the antibiotic- and GF-modified coating are presented in Fig. 3B. The obtained spectra for coating C, coating 4 and coating C/GF appear quite similar, which suggests that the main functional groups remain the same in all samples, and the addition of active substances did not significantly affect the chemical structure of the base matrix. In the case of these multicomponent materials, the disappearance of the aforementioned band at 1635 cm^{-1} is not observed, as there is a strong signal from Amide I in this range, which comes mainly from the stretching vibrations of the C=O bond present in collagen or can be from the peptide bond from glutathione.[28] The strongly prominent peak for coating C at 1023 cm^{-1} belongs to the asymmetric stretch PO_4^{3-}, one of the main phosphate bands characteristic for Hap.[39] In the case of coating C/GF, a slight enhancement of the bands at 1285 cm^{-1} and 1340 cm^{-1} (indicated by the dashed line on the purple spectrum) was observed, which may originate from the Amide III group found in VEGF and TGF-β, a group characteristic of protein structures.[40]

Ceramic-polymer composites can be obtained in a variety of ways including chemical crosslinking, thermal crosslinking or photo-crosslinking. Also the sol–gel method.[41] Compared to these, the photocrosslinking method has some advantages, as it usually takes less time than chemical or sol–gel crosslinking, and does not require high temperatures like thermal crosslinking. However, even though photocrosslinking usually takes a few minutes, it is extremely important to avoid excessive sedimentation of the ceramic phase, therefore, to select the crosslinking and composition parameters in such a way as to obtain a continuous material quickly enough so that one of the phases does not have time to fall off, and the final material obtained shows an even distribution of phases. Determination of the migration front and sedimentation rate of ceramics in polymer solutions allowed to select a polymer composition with optimal viscosity. The results obtained for a 1 : 1 PVP/PEG blend, were consistent with reports of a similar study for PVP.[42] The use of a photocrosslinking process and the selection of the appropriate amount of components or photoinitiator and crosslinking agent, in this case PEGDA, allows control over the physicochemical parameters of the material. The amount of PEGDA affects the mechanical parameters of the material's hardness or elasticity, as well as the kinetics of the release of active substances, as the degree of crosslinking of the material affects the rate of their release.[43] The higher the degree of crosslinking, the less permeable the pores of the hydrogel become, which translates into hindering the process of particle diffusion. In the case of a lower degree of crosslinking, the materials exhibit a greater ability to swell, which facilitates particle diffusion.[44]

The results of the SEM imaging are provided in Fig. 5. The surfaces appear to be similar to each other and no significant differences in structure are observed. The smoother sections in coating C/GF are likely the result of sample preparation for testing, as the coating was removed from the PLLA to examine the coating interior.

The elemental composition of the coatings was determined by EDX microanalysis and expressed as mass percent (m.%) and atomic percent (at.%). These values are presented in Table 3. The table summarizes the elemental content found on the microscopically observed materials. The content of Ca and P is similar in all materials, and their presence is a result of the composition of the HAp used in the coatings as a reinforcing phase. For coating 4, the presence of Cl ions was detected, the origin of which is related to clindamycin. Clindamycin hydrochloride was used hence its presence. The map of Cl distribution in the material confirms that the drug is evenly distributed throughout the material.[45] Also of interest is the detection of S for coating C/GF, the origin of which is probably related to the chemical structure of the VEGF and TGF-β proteins. This element is involved in the formation of disulfide bridges in proteins.[46,47] Although its % content is low relative to the other elements, its even distribution can be observed throughout the volume of the test sample. Additional information on EDX analysis of coatings is presented in the SI (subsection 6).

Fig. 6 presents the amounts of VEGF-165 and TGF-β1 released over 72 h incubation in PBS fluid. The first 24 hours after implant placement are vital for establishing the foundation of healing and integration, influencing the long-term success of biomaterial. In this initial period, a relatively fast

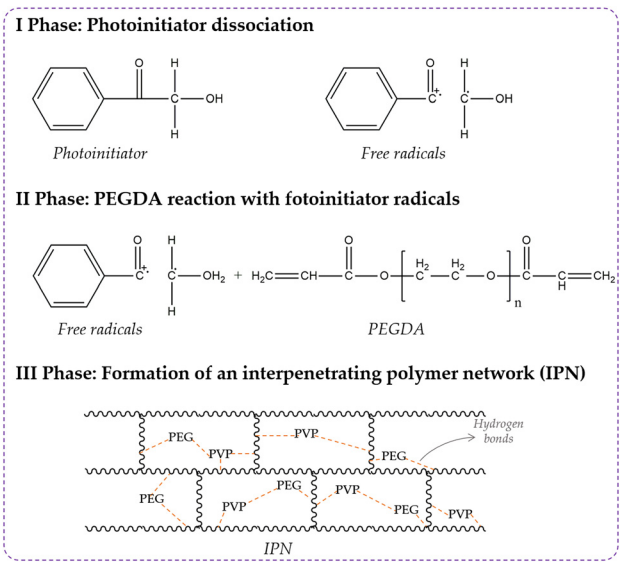

Fig. 4 The proposed mechanism for crosslinking materials.

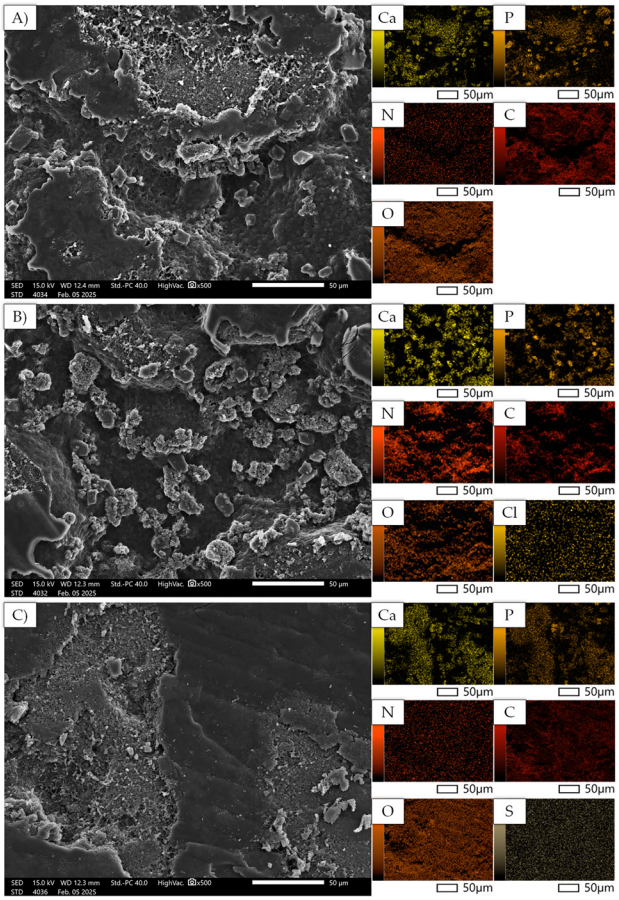

Fig. 5 SEM imaging of the morphology of the samples (A) coating C, (B) coating 4, (C) coating C/GF.

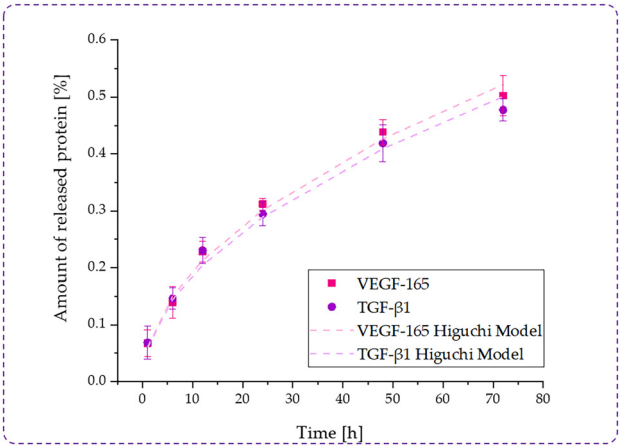

Fig. 6 Cumulative release profiles of VEGF-165 and TGF-β1 from the coating C/GF over 72 h incubation in PBS fluid. Dashed lines represent the Higuchi model fit indicating a diffusion-controlled release mechanism.

release of both incorporated growth factors was observed. The released amounts of VEGF-165 and TGF-β1 are similar and reach 31.2% and 29.5%, respectively. These similar values may be a result of the fact that despite their different properties and parameters, these proteins possess a relatively similar kDa value. TGF-β1 is a 25 kDa polypeptide that consists of two seemingly identical 12.5 kDa subunits linked by disulfide bonds.[48] On the other hand, the size of VEGF-165 is estimated at 23–22 kDa.[49] Given these values, it is likely that the two proteins were able to penetrate the polymer network in a similar manner, migrating between polymer chains.[50]

After the initial burst phase, sustained release was observed, with cumulative release reaching approximately 50.2% for VEGF-165 and 47.7% for TGF-β1 after 72 hours. This biphasic profile, consisting of a rapid initial release followed by a slower, continuous phase, is characteristic of polymer-based delivery systems. The slower phase is likely to result from the diffusion of proteins trapped deeper in the cross-linked polymer matrix and possibly interacting with the hydrogel components.

To better understand the release mechanism, the experimental data were fitted to the Higuchi model which describes drug release governed by Fickian diffusion from a homogeneous matrix.[51] The model provided a good fit to the experimental data for both growth factors, yielding release constants of k = 0.062 (VEGF-165) and k = 0.059 (TGF-β1). These values, together with the curve fit in the graph, confirm that diffusion through the polymer network is the main mechanism driving protein release.[52] Furthermore, the similar release profile for both GFs supports the concept that protein diffusion in this system is primarily influenced by polymer network structure and porosity, rather than specific differences due to protein type.

Previous work has demonstrated that as the proportion of HAp increases, the amount of clindamycin released decreases.

Table 3 Elemental EDX analysis of coatings, summary of mass [%] and atomic [%] amounts of individual elements

	Coating C		Coating 4		Coating C/GF	
Element	Mass [%]	Atom [%]	Mass [%]	Atom [%]	Mass [%]	Atom [%]
Ca	5.99 ± 0.28	2.16 ± 0.10	6.55 ± 0.31	2.38 ± 0.11	6.32 ± 0.26	2.29 ± 0.10
P	2.22 ± 0.14	1.03 ± 0.07	2.16 ± 0.15	1.02 ± 0.07	2.35 ± 0.13	1.10 ± 0.06
N	3.27 ± 0.53	3.37 ± 0.54	4.09 ± 0.59	4.27 ± 0.61	3.60 ± 0.50	3.73 ± 0.51
C	45.30 ± 0.45	54.44 ± 0.55	42.54 ± 0.47	51.70 ± 0.57	44.01 ± 0.42	53.23 ± 0.50
O	43.22 ± 0.97	38.99 ± 0.87	44.44 ± 1.02	40.55 ± 0.93	43.60 ± 0.89	39.59 ± 0.81
Cl	—	—	0.22 ± 0.05	0.09 ± 0.02	—	—
S	—	—	—	—	0.11 ± 0.05	0.74 ± 0.01

As little as 5% addition of ceramic reduced the amount of clindamycin released by about 12% after 24 h incubation in PBS.[32] Considering those reports, in this work, the material exhibiting the greatest application potential (coating C) was modified with growth factors – VEGF-165 and TGF-β1. Naturally, the amount of proteins released will also depend on the original amount used for modification. For this reason, it is rather tough to compare them to other literature reports. However, in the context of the research presented in this paper, the amount released is extremely important in terms of the effective dose of each substance. In the case of VEGF, the therapeutic effect of improving intervascular integrity was observed for doses of 0.1 mg kg^{-1} for intratissue administration and 1.0 mg kg^{-1} for intravenous injection.[53] However, these data are related to doses adjusted for improved renal health. In the case of TGF-β1, on the other hand, biological activity can already be observed at the surprisingly low dose range of 0.1–10 ng mL^{-1}. It is presumed that the reduction in damage to hippocampal CA1 neurons (responsible for cognitive function and memory processes), observed at this amount of protein, may be related to the antioxidant and anti-apoptotic effects of TGF-β1.[54] As little as 0.1 ng mL^{-1} TGF-β1 exhibited the ability to produce cartilage matrix, while material without GF did not show this ability at all.[55] VEGF at a concentration of 120 ng mL^{-1} causes an approximately twofold increase in the expression of osteoblast differentiation genes, *i.e.* alkaline phosphatase (ALP) and collagen I alpha I (COL1α1).[56] Studies conducted in this work have demonstrated that positive changes can also be observed at a much lower dose. In particular, compared to an intravenous dose, the amount of active ingredient released locally may be reduced, as systemic distribution of the compound throughout the body is then avoided.[57]

The analysis of cytokine levels presented in Fig. 7 illustrates the biocompatibility and safety of the tested biomaterials (coating C, coating 4, coating C/GF) applied to animals. Fig. 8 shows the surgical procedure for implantation of polymer-ceramic composites into cranial bone defects in a rat model. The levels of the pro-inflammatory cytokines IL-1β and TNF-α remained consistently low across all experimental groups. This suggests that the tested biomaterials do not activate acute inflammatory pathways, indicating a lack of harmful effects. The levels of IL-10, a cytokine associated with anti-inflammatory activity and tissue repair, remained comparable across groups with only slight variations, indicating that the inflammatory process was effectively modulated. Importantly, the concentrations of all tested cytokines were compared with the values measured in the sera of untreated animals (NTC).

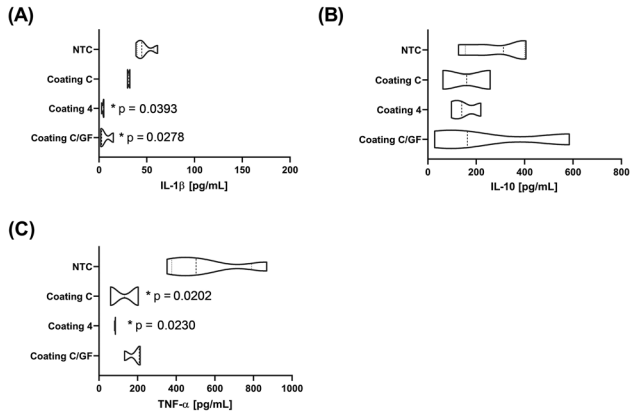

Fig. 7 The concentration of interleukin-1β – IL-1β (A), interleukin-10 – IL-10 (B) and tumor necrosis factor-α – TNF-α (C) in the serum samples obtained from animals after biomaterials implantation. NTC – non-treated control (rats not subjected to implantation of the biomaterials). Number of animals, n = 3. * – statistical significance *vs.* NTC, p value given next to "*".

The next stage of the work involved visualizing the mineralization of the animals' cranial bones at the site of the defect. For this purpose fluorescent dye – Xylenol orange (concentration 25 mg per kg body weight) was injected subcutaneously into the animals 8 weeks after implantation of the tested biomaterials, at 72 hours before euthanasia. The fluorescence signal reflects the incorporation of Xylenol orange dye indicating active bone mineralization sites. The images obtained indicate that the coating C/GF material facilitated the mineralization of the bone areas directly in contact with the implanted material (areas glowing green, Fig. 9A). Skull sections containing the implanted biomaterials were also visualized with a confocal macroscope using the following wavelengths λ = 440/570 – 610 nm for Xylenol orange. The images obtained indicate that the coating C/GF material contributed to significant bone regeneration 8 weeks after implantation compared to the reference material – coating C (area glowing green, Fig. 9A).

Significantly elevated levels of osteopontin (OPN) in the coating 4 and coating C/GF groups further confirmed the microscopic observations (Fig. 9B). OPN is a multifunctional protein crucial in bone healing, particularly in the recruitment and activation of osteoclasts and osteoblasts. Elevated OPN levels in serum indicate active bone remodeling and mineralization processes, underscoring the higher regenerative efficacy of the growth factor-enriched composite.[58–60]

In vivo results suggest that incorporating growth factors: VEGF-165 and TGF-β1 into the composite significantly promoted mineralization at the defect site as evidenced by increased osteopontin (OPN) levels in serum, measured using ELISA, and histological analysis of the explanted cranial bone defects, which revealed enhanced bone matrix deposition and mineralized tissue formation compared to the control groups. Growth factors such as VEGF-165 and TGF-β1 are crucial mediators in the process of bone regeneration and tissue healing. VEGF-165 stimulates angiogenesis by promoting the proliferation and migration of endothelial cells, which leads to the formation of new blood vessels. This is particularly important in bone repair, as an adequate blood supply is essential for delivering oxygen, nutrients, and cells involved in the healing process. In addition to its role in angiogenesis, VEGF-165 enhances osteoblast activity, facilitating the formation of new bone tissue by promoting the differentiation and mineralization of these bone-forming cells.[61,62] Also,

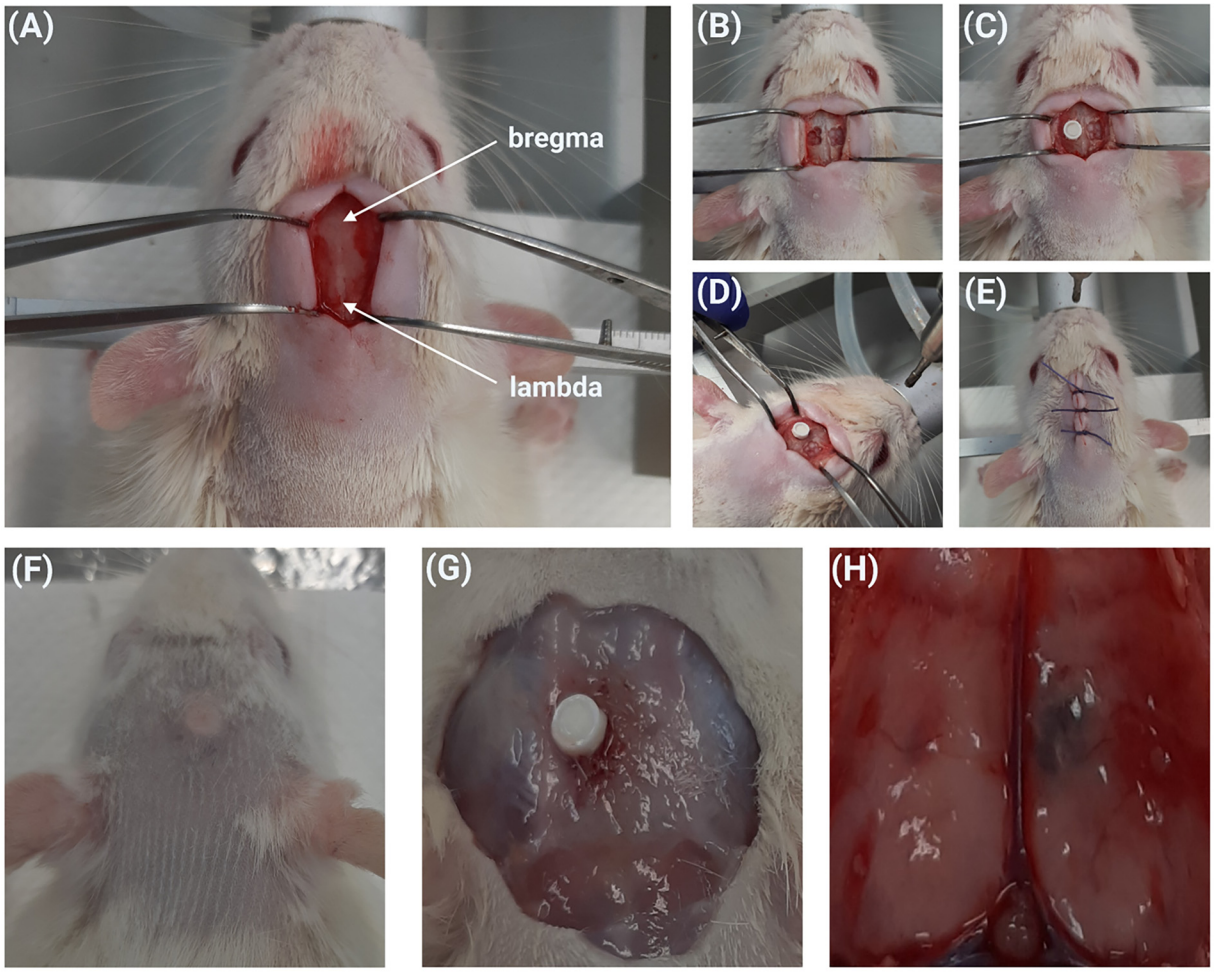

Fig. 8 Steps in the surgical procedure for implantation of polymer-ceramic composites into cranial bone defects in a rat model. (A) Exposure of the calvarial area showing anatomical landmarks (bregma and lambda) for precise defect localization. (B) Creation of a standardized circular defect in the calvarial bone using a trephine drill under sterile conditions. (C and D) Placement of the composite material into the defect site. (E) Closure of the surgical site using sutures to ensure proper healing. (F) Post-operative recovery of the animal under monitoring. (G) Inspection of the defect site during the healing period to assess implant positioning and integration. (H) Visualization of the cranial area showing spontaneous regeneration of the tissue defect without the involvement of an implant.

VEGF released from the composite can play supportive role in bone regeneration by enhancing angiogenesis, as demonstrated by increase tube formation of endothelial cells. This angiogenetic activity alongside upregulated osteogenic and angiogenic biomarkers *in vivo*, contributed to effective bone defect repair.[63] On the other hand, TGF-β1 plays a pivotal role in bone regeneration by regulating several processes in the extracellular matrix. It promotes the deposition of key components such as collagen and proteoglycans, which provide a scaffold for bone tissue development. Furthermore, TGF-β1 stimulates the recruitment and differentiation of mesenchymal stem cells (MSCs) into osteoblasts, enhancing bone formation. It also modulates the activity of osteoclasts to maintain a balanced bone remodeling process.[64–66] Together, these growth factors act synergistically to create an environment conducive to effective bone healing and regeneration.

This study confirmed that the coating contributed to significant bone regeneration 8 weeks after implantation compared to the reference material, and furthermore, the developed coating was demonstrated not to activate acute inflammatory pathways, as confirmed by determining levels of the pro-inflammatory cytokines IL-1β and TNF-α and comparing the obtained values to those of untreated animals. In the case of bone tissue regeneration, many previous studies, such as the work of Zhang *et al.* (2019) or Uskoković and Desai (2014), are often concerned with ceramic-only systems for local delivery of active ingredients.[67,68] Mainly this is HAp, the gold standard in the biomedical field due to its composition and similarity to human bone. However, it is important to consider that the use of composites can significantly improve material properties. Addition of HAp to the composite leads to a highly improved effect on MC3T3 cell differentiation and mineraliz-

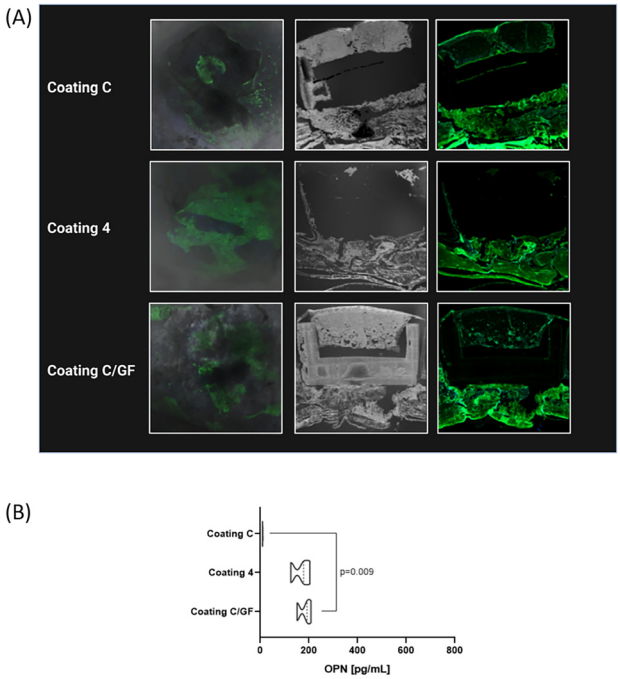

Fig. 9 Representative images of skull sections containing implanted biomaterial illustrating bone mineralization processes after 8 weeks of implantation. The fluorescence signal reflects the incorporation of Xylenol orange dye, administered *in vivo* at 72 hours prior to euthanasia, indicating active bone mineralization sites (A). Serum levels of osteopontin – OPN (B).

ation of the extracellular matrix. Cell differentiation for the ceramic materials was up to twice as high.[69]

Future perspectives

The results presented in this study have important implications for the development of materials engineering aimed at bone tissue regeneration. The developed composite coatings, with their controlled-release properties and synergistic growth factor action, offer a promising solution for bone defects of critical size. The ability to adapt the photocrosslinking process to different shapes and sizes of implants increases its versatility in personalized medicine applications, by tailoring it to individual patient needs. The coating can be used on its own as a more flexible filling, or applied to cover other implants, as demonstrated in this study with composite or polymer structures, as well as 3D-printed component. As a result, solid materials that have no, or very low, biological activity can receive additional functions and important properties. It is also important to note that this approach has the potential to reduce reliance on allo- and autografts, which are associated with donor site morbidity, limited availability, as well as being a potential ethical constraint. From an application perspective, it is also crucial to highlight the sustainable nature of the developed materials. The proposed method of obtaining these coatings is both ecological and economical, as it eliminates the need for toxic solvents and reagents while preventing the generation of hazardous by-products that would otherwise require costly disposal. Environmentally friendly methods of materials synthesis, is an important factor in the context of global sustainability efforts. Minimization of energy consumption as well as reduction of chemical waste are in line with the principles of green chemistry, promoting responsible innovation in regenerative medicine. This environmentally conscious approach not only supports sustainable material development but also have potential to enhance the feasibility of translating these findings into clinical and industrial applications. However, the results presented in the above paper have their limitations, and potential application would be possible with the appropriate steps. The presented solution in the legal sense is a class-three medical device, which must meet the relevant standards as well as regulations. The process would need to be scaled up and translated from the laboratory to a real environment. The coating material has been tested under *in vivo* conditions on animal models in the form of rats, relatively small animals, therefore the model may not fully reflect the actual bone healing process due to anatomical differences. Future studies should consider larger animal models that exhibit greater similarity to humans. The potential to expand the solution, as well as to increase its biological value, is the possibility of modifying the carrier additionally with other active agents, which, acting synergistically to the pre-applied components, could promote tissue regeneration. In the aspect of bone tissue, this could be bone morphogenetic protein (BMP).

Conclusions

The results obtained in this study highlight the significant potential of incorporating growth factors such as VEGF-165 and TGF-β1, and clindamycin into ceramic-polymer composite coatings for bone tissue regeneration. The materials can be customized into a variety of shapes and sizes which increases versatility for personalized medicine applications. The unique solution proposed in the presented work to obtain coatings was the use of a photocrosslinking process in UV light.

In conclusion, the composite coatings developed and presented in this work, obtained by crosslinking and capable of releasing clindamycin and protein growth factors, represent a novel as well as an effective strategy for promoting bone regeneration. This technology potentially may significantly impact orthopaedic and regenerative medicine clinical practice. However, while studies conducted in both *in vitro* and *in vivo* conditions have confirmed safety as well as bioactivity, further research is needed in this context.

Author contributions

Conceptualization: DS; visualization: DS; preparation of materials and material elements: DS, BK; investigation: DS, ASG, MW, AK, KN; supervision: ASK, KR; planning, execution,

and analysis of *in vivo* experiments, ASz-G, MW, and AK; writing—original draft: DS, ASG, MW, AK, BK; writing—review & editing: ASK, KR; resources: ASK, KS, KR; management: ASK, KS, KR; project administration: ASK. All authors have read and agreed to the published version of the manuscript.

Conflicts of interest

There are no conflicts to declare.

Ethical statement

All animal procedures were performed in accordance with the Guidelines for Care and Use of Laboratory Animals of University of Lodz and approved by the Local Ethical Committee for Animal Experiments based at the Medical University of Lod (Protocol No. ŁB192/2021 dated February 8, 2021).

Data availability

Supplementary information: data related to this article, including FTIR measurements, XRD measurements, GF release determination, SEM imaging, EDS microanalysis, as well as stability and sedimentation rate measurements, are available in the Mendeley Data repository at **https://data.mendeley.com/datasets/m9xh8wysc5/1** and the data including cytokine measurements (IL-1β, IL-10, TNF-α and OPN) and representative confocal images, are available in the University of Lodz repository at **https://hdl.handle.net/11089/56178**. See Supplementary information at DOI: **https://doi.org/10.1039/d5bm00637f**.

Acknowledgements

The "Multifunctional biologically active composites for applications in bone regenerative medicine" project was carried out within the TEAM-NET program of the Foundation for Polish Science, financed by the European Union under the European Regional Development Fund (grant number POIR.04.04.00-00-16D7/18). The authors gratefully acknowledge the financial support. The authors would like to express their deep thanks to PhD Wioletta Florkiewicz and PhD Michał Grzymajło for their technical support during the laboratory work. The authors also thank PhD Katarzyna Harazna for her valuable comments and suggestions.

References

1 L. A. Dobrzański, A. D. Dobrzańska-Danikiewicz and L. B. Dobrzański, *Processes*, 2021, **99**(4), DOI: **10.3390/pr9050865**.
2 G. Gautam, S. Kumar and K. Kumar, *Mater. Today: Proc.*, 2022, **50**, 2206–2217.
3 M. A. Markets, *Biomaterials Market by Type (Metallic (Gold, Magnesium), Ceramic (Aluminum Oxide, Carbon), Polymer (Polyethylene, Polyester), Natural (Hyaluronic acid, Collagen, Gelatin)), Application (Orthopedic, Dental, CVD, Ophthalmology) & Region - Global Forecast to*, 2024.
4 Z. U. Arif, M. Y. Khalid, M. F. Sheikh, A. Zolfagharian and M. Bodaghi, *J. Environ. Chem. Eng.*, 2022, **10**(4), DOI: **10.1016/j.jece.2022.108159**.
5 M. Yang, L. Chen, J. Wang, G. Msigwa, A. I. Osman, S. Fawzy, D. W. Rooney and P. S. Yap, *Environ. Chem. Lett.*, 2023, **21**, 55–80.
6 E. Asadian, S. Abbaszadeh, F. Ghorbani-Bidkorpeh, S. Rezaei, B. Xiao, H. A. Santos and M. A. Shahbazi, *Biomater. Sci.*, 2024, 9–92.
7 Z. Abbas, M. Dapporto, A. Tampieri and S. Sprio, *J. Compos. Sci.*, 2021, **5**(10), 259.
8 C. I. Idumah, *Polym. Polym. Compos.*, 2021, **29**, 509–527.
9 F. Nudelman and R. Kröger, *Science*, 2022, **376**, 137–138.
10 M. Liu, Y. Wang, X. Liu, Q. Wei, C. Bao and K. Zhang, *ACS Biomater. Sci. Eng.*, 2023, **9**, 3032–3057.
11 M. Zhang, J. Liu, T. Zhu, H. Le, X. Wang, J. Guo, G. Liu and J. Ding, *ACS Appl. Mater. Interfaces*, 2022, **14**, 1–19.
12 F. Wei, G. Liu, Y. Guo, R. Crawford, Z. Chen and Y. Xiao, *Biomater. Sci.*, 2018, **8**, 2156–2171.
13 W. Liang, X. Wu, Y. Dong, R. Shao, X. Chen, P. Zhoud and F. Xu, *Biomater. Sci.*, 2021, **6**, 1924–1944.
14 D. Qin, N. Wang, X.-G. You, A.-D. Zhang, X.-G. Chen and Y. Liu, *Biomater. Sci.*, 2022, **2**, 318–353.
15 K. Jahan and M. Tabrizian, *Biomater. Sci.*, 2016, **4**, 25–39.
16 A. Dubey, S. Jaiswal and D. Lahiri, *ACS Biomater. Sci. Eng.*, 2022, **8**, 1001–1027.
17 E. Tahmasebi, M. Alam, M. Yazdanian, H. Tebyanian, A. Yazdanian, A. Seifalian and S. A. Mosaddad, *J. Mater. Res. Technol.*, 2020, **9**, 11731–11755.
18 M. E. Brassesco, J. Cortez, V. Triacca, J. Payen and Y. Bayon, *ACS Biomater. Sci. Eng.*, 2024, **10**, 1910–1920.
19 H. A. Rather, D. Jhala and R. Vasita, *Mater. Sci. Eng. C*, 2019, **103**, 109761.
20 A. Gilarska, A. Hinz, M. Bzowska, G. Dyduch, K. Kamiński, M. Nowakowska and J. Lewandowska-Łańcucka, *ACS Appl. Mater. Interfaces*, 2021, **13**, 49762–49779.
21 C. Rastogi, H. T. Rube, J. F. Kribelbauer, J. Crocker, R. E. Loker, G. D. Martini, O. Laptenko, W. A. Freed-Pastor, C. Prives, D. L. Stern, R. S. Mann and H. J. Bussemaker, *Science*, 2021, **373**, E3692–E3701.
22 Y. Wu, R. Fu, S. Mohanty, M. Nasser, B. Guo and G. Ghosh, *ACS Appl. Bio Mater.*, 2019, **2**, 2339–2346.
23 A. Halim, H. C. Kuo and P. S. Hou, *Discover Neurosci.*, 2025, **20**, 3.
24 B. Aksan and D. Mauceri, *J. Biomed. Sci.*, 2025, **32**, 1–21.
25 E. Kardalas, E. Sakkas, M. Ruchala, D. Macut and G. Mastorakos, *Rev. Endocr. Metab. Disord.*, 2022, **23**, 431–447.

26 X. Lin, S. Patil, Y. G. Gao and A. Qian, *Front. Pharmacol.*, 2020, **11**, 1–15.
27 B. Kryszak, M. Biernat, P. Tymowicz-Grzyb, A. Junka, M. Brożyna, M. Worek, P. Dzienny, A. Antończak and K. Szustakiewicz, *Polymer*, 2023, **287**, 126428.
28 A. M. Tomala, D. Słota, W. Florkiewicz, K. Piętak, M. Dyląg and A. Sobczak-Kupiec, *Lubricants*, 2022, **10**, 58.
29 D. Słota, J. Jampilek and A. Sobczak-Kupiec, *J. Funct. Biomater.*, 2024, **15**, 1–18.
30 Thermo Fisher Scientific. *Human TGF-β1 ELISA Kit user guide (Pub. No. MAN0016624 Rev. A.0). From Thermo Fisher Scientific website*: **https://assets.thermofisher.cn/TFS-Assets%2FLSG%2Fmanuals%2FMAN0016624-249-4-Hu-TGF-beta1-ELISA-UG.pdf**.
31 Thermo Fisher Scientific. *Human VEGF ELISA Kit product information sheet (Pub. No. MAN0003960 Rev. 3.0). From Thermo Fisher Scientific website*: **https://tools.thermofisher.com/content/sfs/manuals/KHG0111_Hu_VEGF_ELISA_Rev2.pdf**.
32 D. Słota, M. M. Urbaniak, A. Tomaszewska, K. Niziołek, M. Włodarczyk, W. Florkiewicz, A. Szwed-Georgiou, A. Krupa and A. Sobczak-Kupiec, *Biomater. Sci.*, 2024, (20), 5253–5265.
33 M. Chen, R. Aluunmani, G. Bolognesi and G. T. Vladisavljević, *Molecules*, 2023, **99**(10), 2341.
34 M. Hakim Khalili, R. Zhang, S. Wilson, S. Goel, S. A. Impey and A. I. Aria, *Polymers*, 2023, **15**, 2341.
35 H. M. Zidan, E. M. Abdelrazek, A. M. Abdelghany and A. E. Tarabiah, *J. Mater. Res. Technol.*, 2019, **8**, 904–913.
36 C. Cona, K. Bailey and E. Barker, *Polymers*, 2024, **16**(14), 2050.
37 D. K. Thukral, S. Dumoga, S. Arora, K. Chuttani and A. K. Mishra, *Cancer Nanotechnol.*, 2014, **5**, 1–15.
38 F. Khan, M. Atif, M. Haseen, S. Kamal, M. S. Khan, S. Shahidc and S. A. A. Nami, *J. Mater. Chem. B*, 2022, 170–203.
39 D. K. Khajuria, V. B. Kumar, D. Gigi, A. Gedanken and D. Karasik, *ACS Appl. Mater. Interfaces*, 2018, **10**, 19373–19385.
40 M. Mitra, M. H. Sanfui, S. Roy, M. Deb, C. Roy, A. Dutta, N. N. Ghosh, M. Rahaman, P. K. Chattopadhyay, S. Roy and N. R. Singha, *Macromolecules*, 2023, **56**, 9078–9096.
41 M. Shahbazi, S. J. Ahmadi, A. Seif and G. Rajabzadeh, *Food Hydrocolloids*, 2016, **61**, 378–389.
42 M. Głab, S. Kudłacik-Kramarczyk, A. Drabczyk, J. Walter, A. Kordyka, M. Godzierz, R. Bogucki, B. Tyliszczak and A. Sobczak-Kupiec, *Molecules*, 2021, **26**(14), 4268.
43 W. X. Wu, Y. C. Huang and W. F. Lee, *Iran. Polym. J.*, 2020, **29**, 679–691.
44 M. J. L. Dantas, B. F. F. Santos, A. A. Tavarez, M. A. Maciel, B. M. Lucena, M. V. Fook and S. M. Silva, *Molecules*, 2019, **24**, 1–20.
45 P. J. Weldrick, S. San and V. N. Paunov, *ACS Appl. Nano Mater.*, 2021, **4**, 1187–1201.
46 V. Manuelli, C. Pecorari, G. Filomeni and E. Zito, *FEBS J.*, 2022, **289**, 5413–5425.
47 M. V. Lukassen, C. Scavenius, I. B. Thøgersen and J. J. Enghild, *Biochemistry*, 2016, **55**, 5610–5621.
48 Z. Deng, T. Fan, C. Xiao, H. Tian, Y. Zheng, C. Li and J. He, *Signal Transduction Targeted Ther.*, 2024, **9**(1), 61.
49 I. Inoki, T. Shiomi, G. Hashimoto, H. Enomoto, H. Nakamura, K. Makino, E. Ikeda, S. Takata, K. Kobayashi and Y. Okada, *FASEB J.*, 2001, **16**(2), 1–27.
50 Y. Tang, X. Zhang, X. Li, C. Ma, X. Chu, L. Wang and W. Xu, *Eur. Polym. J.*, 2022, **162**, 110881.
51 D. R. Paul, *Int. J. Pharm.*, 2011, **418**, 13–17.
52 J. Siepmann and N. A. Peppas, *Int. J. Pharm.*, 2011, **418**, 6–12.
53 J. P. Waller, S. P. Burke, J. Engel, A. R. Chade and G. L. Bidwell, *Sci. Rep.*, 2021, **11**, 1–15.
54 P. Henrich-Noack, J. H. M. Prehn and J. Krieglstein, *Stroke*, 1996, **27**, 1609–1615.
55 X. Ju, X. Liu, Y. Zhang, X. Chen, M. Chen, H. Shen, Y. Feng, J. Liu, M. Wang and Q. Shi, *Smart Mater. Med.*, 2022, 85–93.
56 B. Divband, M. Aghazadeh, Z. H. Al-qaim, Z. Haleem, M. Samiei, F. H. Hussein, A. Shaabani, S. Shahi and R. Sedghi, *Carbohydr. Polym.*, 2021, 118589.
57 S. G. Antimisiaris, A. Marazioti, M. Kannavou, E. Natsaridis, F. Gkartziou, G. Kogkos and S. Mourtas, *Adv. Drug Delivery Rev.*, 2021, **174**, 53–86.
58 D. E. Rodriguez, T. Thula-mata, E. J. Toro, Y. Yeh, C. Holt, S. Holliday and L. B. Gower, *Acta Biomater.*, 2014, **10**, 494–507.
59 S. Bolamperti, I. Villa and A. Rubinacci, *Bone Res.*, 2022, **10**(1), 48.
60 M. Nagao, T. N. Feinstein, Y. Ezura, T. Hayata, T. Notomi, Y. Saita, R. Hanyu, H. Hemmi, Y. Izu, S. Takeda, K. Wang, S. Rittling, T. Nakamoto, K. Kaneko, H. Kurosawa, G. Karsenty, D. T. Denhardt, J. P. Vilardaga and M. Noda, *Proc. Natl. Acad. Sci. U. S. A.*, 2011, **108**, 17767–17772.
61 K. Hu and B. R. Olsen, *Bone*, 2016, **91**, 30–38.
62 S. Tong, D. P. Xu, Z. M. Liu, Y. Du and X. K. Wang, *J. Craniofacial Surg.*, 2016, **27**, 509–515.
63 C. Huang, S. Shi, M. Qin, X. Rong, Z. Ding, X. Fu, W. Zeng, L. Luo, D. Wang, Z. Luo, Y. Li and Z. Zhou, *Adv. Sci.*, 2024, **11**, 1–18.
64 W. Mengruii, W. Shali, C. Wei and L. Yi-Ping, *Cell Res.*, 2024, **34**, 101–123.
65 M. N. Labour, M. Riffault, S. T. Christensen and D. A. Hoey, *Sci. Rep.*, 2016, **6**, 1–13.
66 S. Kasagi and W. Chen, *Cell Biosci.*, 2013, **3**, 1–7.
67 K. Zhang, Y. Zhou, C. Xiao, W. Zhao, H. Wu, J. Tang, Z. Li, S. Yu, X. Li, L. Min, Z. Yu, G. Wang, L. Wang, K. Zhang, X. Yang, X. Zhu, C. Tu and X. Zhang, *Sci. Adv.*, 2019, **5**, 1–16.
68 V. Uskoković and T. A. Desai, *Mater. Sci. Eng. C*, 2014, **37**, 210–222.
69 P. Jiang, Y. Zhang, R. Hu, X. Wang, Y. Lai, G. Rui and C. Lin, *Bioact. Mater.*, 2021, **6**, 1118–1129.